ADMISSIBLE SHAPE PARAMETERS FOR A PLANAR QUASI-STATIC CONSTRAINT MODE TIRE MODEL

Rui Ma[a]
John B. Ferris[a]
Alexander A. Reid[b]
David Gorsich[b]

[a] Vehicle Terrain Performance Laboratory, Virginia Tech Mechanical Engineering Department

[b] US Army Tank Automotive Research, Development and Engineering Center (TARDEC)

ABSTRACT

The interaction between the tire and terrain has long been of interest for vehicle dynamic simulation. Detailed tire models produce accurate results, but are too computationally intensive for the iterative vehicle design process. The objective of this work is to develop a computationally efficient way to estimate the tire's deformed shape, from which the tire forces can be evaluated. A novel, planar, quasi-static, constraint mode tire model is developed to address this objective. The required model parameters are reduced to two non-dimensional shape parameters and an overall stiffness factor. An admissible domain of the shape parameters is developed based on the deformation limitations of a physical tire. Specifically, no single harmonic may dominates the tire shape and the low spatial frequency components must contribute more than higher frequency components to the overall tire shape. The ability of the model to accurately predict the spindle force is evaluated by comparing simulation and experimental responses for quasi-static flat plate and cleat tests. This work provides a simple, accurate tire model for circumferential displacement and vertical spindle force prediction to improve the vehicle design process.

Keywords: Terrain Surface, Planar Tire Model, Constraint Mode

NOMENCLATURE

N Total number of tire segments

u Radial deflection.

R Tire radius.

F_n Radial force acting on n^{th} tire segment.

F Vertical spindle force.

f Linearly distributed load density.

κ Radial stiffness density.

U_b Bending potential energy for each tire segment.

M Bending moment for each tire segment.

E Elastic modulus.

I Second moment of inertia for each tire segment.

U_s Shear potential energy for each tire segment.

G Shear modulus.

A Cross-sectional area.

U_e Elastic potential energy for each tire segment.

1. REPORT DATE **21 JAN 2014**	2. REPORT TYPE **Journal Article**	3. DATES COVERED **11-04-2013 to 28-12-2013**	
4. TITLE AND SUBTITLE **ADMISSIBLE SHAPE PARAMETERS FOR A PLANAR QUASI-STATIC CONSTRAINT MODE TIRE MODEL**		5a. CONTRACT NUMBER	
		5b. GRANT NUMBER	
		5c. PROGRAM ELEMENT NUMBER	
6. AUTHOR(S) **Rui Ma; John Ferris; Alexander Reid; David Gorsich**		5d. PROJECT NUMBER	
		5e. TASK NUMBER	
		5f. WORK UNIT NUMBER	
7. PERFORMING ORGANIZATION NAME(S) AND ADDRESS(ES) **Vehicle Terrain performance laboratory,Virginia Tech Mechanical Engineering Department,635 Prices Fork Road - MC 0238,Blacksburg,VA,24061**		8. PERFORMING ORGANIZATION REPORT NUMBER **; #24409**	
9. SPONSORING/MONITORING AGENCY NAME(S) AND ADDRESS(ES) **U.S. Army TARDEC, 6501 East Eleven Mile Rd, Warren, Mi, 48397-5000**		10. SPONSOR/MONITOR'S ACRONYM(S) **TARDEC**	
		11. SPONSOR/MONITOR'S REPORT NUMBER(S) **#24409**	

12. DISTRIBUTION/AVAILABILITY STATEMENT
Approved for public release; distribution unlimited

13. SUPPLEMENTARY NOTES
For JOURNAL OF DYNAMIC SYSTEM MEASUREMENT AND CONTROL

14. ABSTRACT
The interaction between the tire and terrain has long been of interest for vehicle dynamic simulation. Detailed tire models produce accurate results, but are too computationally intensive for the iterative vehicle design process. The objective of this work is to develop a computationally efficient way to estimate the tire?s deformed shape, from which the tire forces can be evaluated. A novel, planar, quasi-static, constraint mode tire model is developed to address this objective. The required model parameters are reduced to two non-dimensional shape parameters and an overall stiffness factor. An admissible domain of the shape parameters is developed based on the deformation limitations of a physical tire. Specifically, no single harmonic may dominates the tire shape and the low spatial frequency components must contribute more than higher frequency components to the overall tire shape. The ability of the model to accurately predict the spindle force is evaluated by comparing simulation and experimental responses for quasi-static flat plate and cleat tests. This work provides a simple, accurate tire model for circumferential displacement and vertical spindle force prediction to improve the vehicle design process.

15. SUBJECT TERMS
Terrain Surface, Planar Tire Model, Constraint Mode

16. SECURITY CLASSIFICATION OF:			17. LIMITATION OF ABSTRACT **Public Release**	18. NUMBER OF PAGES **14**	19a. NAME OF RESPONSIBLE PERSON
a. REPORT **unclassified**	b. ABSTRACT **unclassified**	c. THIS PAGE **unclassified**			

U_w External work on each tire segment.

γ_1 Distributed physical bending stiffness.

γ_2 Distributed physical shear stiffness.

γ_3 Distributed physical radial stiffness.

k_0 Overall model stiffness.

$\alpha_{1,}\alpha_2$ Model shape parameters.

INTRODUCTION

With the advent of autonomous vehicles and the simultaneous pressure to improve energy efficiency, there are ever increasing demands on vehicle engineers. Clearly there are more electronic and mechatronic systems, more sensors and more actuators. Batteries increase vehicle weight at the same time that the incentive to improve fuel economy continues to grow, which in turn drives a reduction in the overall vehicle weight. These new technologies are making vast improvements in vehicle performance and the way drivers think of their vehicles. They also introduce new challenges to vehicle engineers.

The chassis engineer is faced with numerous design challenges (weight, cost, ride, handling, noise, reliability, packaging…) while interacting with several influential groups (scientific labs, proving ground, suppliers, safety, manufacturing, powertrain and body groups) that result in a highly iterative design process. All these challenges and groups must be satisfied, to the best of the engineer's ability, within a very short timeframe. Within this cacophony of ever-changing requirements and influential groups, some fundamental physical truths remain. Regardless of how the power is developed, or how the wheels are steered, all the vehicle forces must ultimately be reacted through the vehicle suspension and tires. The focus of this work is the interaction between the tires and the main excitation to the vehicle: the terrain [1].

This work addresses the means by which non-deformable terrain imposes a unilateral geometric boundary constraint on rolling tires to which the chassis responds by generating loads, moments, motions, deformations, etc. The terrain surface remains a consistent excitation to the vehicle throughout the iterative design process. Understanding and properly modeling this interaction is critical in predicting the loads and the resulting vehicle performance. However, actual loads are only available at the conclusion of the design and development process when it is difficult and expensive to make modifications.

Clearly, computationally efficient and accurate vehicle dynamic simulations are critical throughout this iterative process. High fidelity, but computationally intensive models that provide very accurate information after the parts have been released are of no use. Simulation results arising from overly simplified models that cannot be trusted and have little value. This work aims to strike a balance between heuristic tire models (such as a linear point-follower) that lack the fidelity to make accurate chassis load predictions and computationally intensive models that cannot provide timely predictions.

The objective of this work is to develop a computationally efficient, planar tire model that accurately predicts the lower-frequency, but not necessarily low amplitude, tire shape. The emphasis is intentionally placed on the shape of the deformed tire, which must be capable of representing the bridging property (over narrow cracks in the pavement) and enveloping property (over sharp bumps). This scope includes relatively large deformations, approaching, but not including, the point of rim strike (when the tire sidewall is folded such that the upper portion is in direct contact with the lower portion and there is a discontinuous and dramatic increase in apparent stiffness). A simple linear relationship between the tire circumferential deformation and the spindle load prediction is used to develop the deformed tire shape with the understanding that more complex force-deflection relationships could be developed using this deformed shape as an initial approximation.

Higher-frequency dynamics such as those that would be required for noise predictions are outside the scope of this work. The focus is the deformed shape of the tire in the region of the contact patch. The majority of the tire is non-contacting and must adopt a smooth shape. That is, the tire model parameterization must be such that the deformed tire shape does not exhibit higher frequency dynamics that are typically associated with higher free-vibration normal modes. Defining the parameter constraints such that these higher order dynamics are omitted is one of the major contributions of this work. This results in the development of an admissible region for the tire shape parameters.

Developing a parsimonious parameter set is one of the major contributions of this work. The tire model developed in this work is completely parameterized by three parameters: a single stiffness parameter and two shape parameters. Experimental data is used to validate the approach using two quasi-static tests, a flat plate and a cleat test, with relatively large deformations. The model is capable of bridging or enveloping small irregularities in the terrain surface and generating the correct tire shape over irregular terrain.

The remainder of this work is developed as follows. Some background on planar tire modeling and the use of constraint modes is briefly reviewed. The mathematical derivation of the constraint mode model is developed such that the entire model can be described by just three parameters. The constraints on the tire shape parameters are developed based on the required physical properties of a tire and the requirement that the shape of the non-contacting region of the tire must be smooth. Finally, the parameterization process for a specific tire is developed and validated with quasi-static experimental results.

BACKGROUND

A considerable amount of tire modeling research has been conducted and a comprehensive review of the current state of the art is presented by Umsrithong [2]. Although a complete review of recent developments is not presented herein, the results from several of these works have direct relevance to the objectives of this study. For example, Badalamenti et al. showed that a radial spring tire model, in which the radial spring element deflection depends on the adjacent element deflections, could accurately describe the tire enveloping behavior in an efficient model [3]. Presently, a planar ring model with an elastic foundation that emphasizes the circumferential deformation is developed to accurately and efficiently describe the tire enveloping behavior.

The deformed shape of the tire (including bridging and enveloping) was accurately predicted by Zegelaar and Pacejka by using a flexible ring to simulate the quasi-static response of a tire rolling over an uneven surface [4]. Although the simulation results agreed with the experimental data, the complexity of the model requires additional computational requirements. The objective to verify the parameter identification process via the deformed shape of the tire is accomplished using experimental, single point-load testing. This single point excitation to the tire model is also used analyze the frequency content of the deformed shape of the tire. Presently, single point-load experimental results are used to parameterize the constraint mode tire model developed in this work. A similar approach was developed by Loo, who modeled the tire by using a more complex flexible circular ring under tension with a nest of linear springs and dampers arranged radially and experimentally identified the parameters using single point-load tests [5]. However in Loo's study the ring tension and foundation stiffness requires contact patch measurements.

It is assumed in this work that the low-frequency deformation of the tire shape can be adequately defined by the quasi-static constraint modes. This assumption is given some credence by Gillespie's study in which a radial spring model is used to simulate the stiffness variation circumferentially and the magnitude of the radial force variation is found to be relatively independent of speed [6]. It is further assumed in this work that the transient response can be adequately represented with a mass-spring tire model. Takayama et al. develops such a model to predict the transient response of a tire encountering a cleat, where the belt and tread region is modeled by a rigid ring and deflections from the cleat are absorbed by a linear and planar spring attached to the rigid ring [7].

Ferris demonstrates that a static constraint mode tire model can be used to capture the tire enveloping and bridging properties with an axisymmetric and circumferentially isotropic model [8]. It is modeled as an inextensible, but flexible, ring supported by an elastic foundation represented by the radial stiffness, κ, as shown in Figure 1a. The tire is divided into N segments and each segment is considered an Euler elastic beam of length $2\pi R/N$ and cross-sectional area, A, shown as a shaded region in Figure 1b. The radial deflection vector $\{u\}$ is used to describe the circumferential tire displacement of each tire segment. The quasi-static constraint modes are developed from Equation (1).
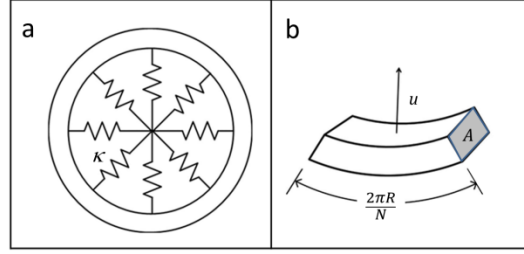
Figure 1. Schematic plot of constraint tire model and a piece of tire segment

$$[K]\{u\} = \{F\} \tag{1}$$

The physical degrees of freedom are categorized into active and omitted sets, represented by superscripts 'a' and 'o' respectively. In general, the boundary degrees of freedom must be a subset of the active degrees of freedom. In the tire modeling case, the active degrees of freedom must include those in contact with the terrain. Therefore the mass and stiffness matrices can be reordered and partitioned as given in equation (2).

$$\begin{bmatrix} [K^{aa}] & [K^{ao}] \\ [K^{oa}] & [K^{oo}] \end{bmatrix} \begin{Bmatrix} \{u^a\} \\ \{u^o\} \end{Bmatrix} = \begin{Bmatrix} \{F^a\} \\ \{0\} \end{Bmatrix} \tag{2}$$

An iterative process to identify the active constraints at the tire-terrain interface is formulated, as shown by Figure 2, beginning with the undeformed tire shape shown in Figure 2(a). The segment with the largest interference is considered the first active constraint, $\{u^a\}$ shown as a single small circle in Figure 2(b). The omitted constraint vector $\{u^o\}$ can be obtained as Equation 3 through Guyan mode reduction [9].

$$\{u^o\} = -[K^{oo}]^{-1}[K^{oa}]\{u^a\} \tag{3}$$

The resulting circumferential deformation with the first active constraint is predicted, as shown in Figure 2(b) where the active constraint is indicated by a small circle. The segment with the most interference in Figure 2(b) is selected as the second active constraint and a new tire shape is computed as shown in Figure 2(c). This process proceeds until there is negligible interference, as shown by Figure 2(f).
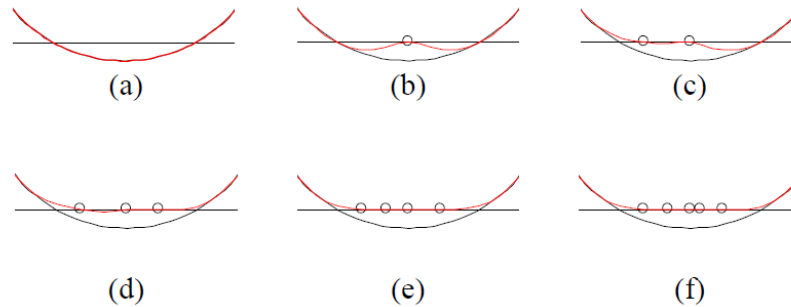

Figure 2. The iterative process to identify the active constraints

The objective of this work is to properly define this stiffness matrix $[K]$. The stiffness matrix is defined with a few parameters (i.e., one stiffness and two shape parameters) and gives reasonable shape predictions for relatively large deflections. Perhaps most importantly, the resulting model yields shapes that are intuitive; the tire shape follows the contour of the terrain along the contact area and is smooth in the non-contacting region of the tire.

MODEL DEVELOPMENT

The quasi-static equation resulting from the application of Hamilton's principle for one tire segment is written as Equation (4).

$$\int_{t_1}^{t_2} (\delta U_b - \delta U_e - \delta U_s + \delta U_w) dt = 0 \qquad \forall t_1, t_2 \tag{4}$$

The virtual changes are computed as Equations (4) - (8).

$$\delta U_b = \frac{2\pi R}{N} EI \frac{\partial^4 u}{\partial x^4} \delta u \tag{5}$$

$$\delta U_e = \frac{2\pi R}{N} \kappa u \delta u \tag{6}$$

$$\delta U_s = \frac{2\pi R}{N} GA \frac{\partial^2 u}{\partial x^2} \delta u \tag{7}$$

$$\delta U_w = \frac{2\pi R}{N} f \delta u \tag{8}$$

The equation of motion for each segment is then simplified to Equation (9).

$$EI \frac{\partial^4 u}{\partial x^4} + \kappa u + GA \frac{\partial^2 u}{\partial x^2} = f \tag{9}$$

For simplicity, the following parameters are defined in Table 1. The tire stiffness parameters (γ_1, γ_2 and γ_3) are invariant for a specific tire; the stiffness associated with a particular tire segment is a function of the number of tire segments, N. It should be clear that each of the three physical stiffness parameters must be positive.

Table 1. Physical stiffness parameters as a function of physical properties

$\gamma_1 = EI(2\pi R)^{-3}$	Segment bending stiffness
$\gamma_2 = GA(2\pi R)^{-1}$	Segment shear stiffness
$\gamma_3 = \kappa(2\pi R)$	Segment radial stiffness
$F_n = \frac{f}{N}(2\pi R)$	Radial force on n^{th} tire segment

The fourth spatial derivative of u for the nth tire segment is approximated by adjacent points via a finite difference method as given in Equation (10).

$$u_n'''' \simeq \frac{u_{n-2} - 4u_{n-1} + 6u_n - 4u_{n+1} + u_{n+2}}{\left(\frac{2\pi R}{N}\right)^4} \tag{10}$$

The equation of motion for the nth tire segment is expressed as Equation (11),

$$k_0\alpha_2 u_{n-2} + k_0\alpha_1 u_{n-1} + k_0 u_n + k_0\alpha_1 u_{n+1} + k_0\alpha_2 u_{n+2} = F_n \tag{11}$$

where the stiffness and shape parameters are defined in terms of the tire parameters as Equation (12) [10].

$$k_0 = 6\gamma_1 N^3 - 2\gamma_2 N + \gamma_3 N^{-1},$$
$$k_0\alpha_1 = \gamma_2 N - 4\gamma_1 N^3, \tag{12}$$
$$k_0\alpha_2 = \gamma_1 N^3$$

The symmetry of a physical tire results in a circulant stiffness matrix $[K]$ that comprises two parts: k_0 defines the overall stiffness and shape matrix $[\alpha]$ defines the relative deformations (i.e., the shape) of the deformed tire [10], as shown in Equation (13).

$$[K] = k_0 \begin{bmatrix} 1 & \alpha_1 & \alpha_2 & 0 & \cdots & \alpha_2 & \alpha_1 \\ \alpha_1 & 1 & \alpha_1 & \alpha_2 & \cdots & 0 & \alpha_2 \\ \alpha_2 & \alpha_1 & 1 & \alpha_1 & \vdots & 0 & 0 \\ 0 & \alpha_2 & \alpha_1 & 1 & \cdots & 0 & 0 \\ \vdots & \vdots & \vdots & \vdots & \vdots & \vdots & \vdots \\ \alpha_1 & \alpha_2 & 0 & 0 & \cdots & \alpha_1 & 1 \end{bmatrix} = k_0[\alpha] = k_0 circ(\{a_i\}) \tag{13}$$

In general, a circulant matrix is denoted by $circ$ and characterized by the first row of the matrix, written as the characteristic row vector $\{a_i\}$. The shape matrix $[\alpha]$ has a circulant form that is only a function of two shape parameters (α_1 and α_2) so that the characterization vector becomes

$$\{a_i\} = \begin{bmatrix} a_0 & a_1 & a_2 & \cdots & a_{\frac{N}{2}-1} \end{bmatrix} = \begin{bmatrix} 1 & \alpha_1 & \alpha_2 & 0 & \cdots & 0 \end{bmatrix} \tag{14}$$

ADMISSIBLE REGION FOR SHAPE PARAMETERS

Clearly the physical tire stiffnesses must be positive and the constraints on the physical stiffnesses must be enforced on the model parameters. It should also be intuitive that the non-contacting region of a tire under quasi-static conditions must adopt a smooth, unrippled shape. That is, the upper section of the tire remains nearly round. More specifically, changes in the radial deformation of the tire occur smoothly and in small increments in the circumferential direction. This implies that the contributions of higher spatial frequencies must remain small. This is in contrast to the deformed shape that a tire assumes when it is being harmonically excited, particularly in the free vibration mode. The remainder of this section proceeds as follows. First the physical restrictions on the tire's stiffness parameters are used to develop a set of constraints on the shape parameters. Next, a single point load is considered in order to develop the spatial frequency constraints. The low-frequency spatial constraint is formulated and the resulting constraints on the shape parameters are developed. This set of constraints forms the admissible region for the shape parameters.

Physical Constraints

The tire shape is constrained by its physical properties which must be enforced as constraints on the shape parameters α_1 and α_2. An admissible region of the shape parameter set is derived from these constraints. Specifically, the tire must possess positive bending, shear and radial stiffness so that the tire stiffness parameters, $\gamma_1 N^3$, $\gamma_2 N$, and $\gamma_3 N^{-1}$ (as shown in Table 1), must be positive. The positive sense for the deflections and corresponding forces are defined such that the overall tire stiffness, k_0 must also be positive. Therefore, the relationships developed in Equation (12) are rearranged to develop constraints on the tire shape parameters, α_1 and α_2, as given in Equation (15).

$$\alpha_2 = \frac{\gamma_1 N^3}{k_0} > 0$$

$$\alpha_1 + 4\alpha_2 = \frac{\gamma_2 N}{k_0} > 0 \tag{15}$$

$$2\alpha_1 + 2\alpha_2 + 1 = \frac{\gamma_3 N^{-1}}{k_0} > 0$$

Next an additional constraint that enforces the low spatial frequency requirement (smoothness for the non-contacting region of the tire) is formulated by considering the effects of a single point load.

Quasi-Static Point Loading

Consider a single point load on the tire such that only one degree of freedom is active. Without loss of generality, the indices of the degrees of freedom are assigned such that this active point is the first degree of freedom. The deformed tire shape is simply computed as Equation (16).

$$\{u\} = \begin{Bmatrix} u^a \\ u^o \end{Bmatrix} = [K]^{-1} \begin{Bmatrix} F^a \\ \emptyset \end{Bmatrix} = [\alpha]^{-1} \begin{Bmatrix} k_0^{-1} F^a \\ \emptyset \end{Bmatrix} \tag{16}$$

Since there is only one active segment, u^a and $k_0^{-1} F^a$ are scalar values and the deformed shape of the tire, $\{u\} = \begin{Bmatrix} u^a \\ u^o \end{Bmatrix}$, is the product of the first column of the matrix $[\alpha]^{-1}$ and the scalar $k_0^{-1} F^a$. To compute the inverse matrix, $[\alpha]^{-1}$, an eigen-decomposition method is applied to the original shape matrix $[\alpha]$. The eigenvalues of the shape matrix $[\alpha]$ are written in vector form as $\{\lambda\}$ and are calculated by applying the Discrete Fourier Transform to the vector $\{a\}$ as shown in Equation (17) [11].

$$\{\lambda\} = \mathcal{F}(\{a\})$$

$$\lambda_k = \sum_{i=0}^{N-1} a_i W^{ik} \qquad k = 0,1,2,\dots,N-1 \tag{17}$$

$$W = e^{-\frac{2\pi}{N}j}$$

The eigenvector corresponding to the kth eigenvalue, $\boldsymbol{v}_k$, is given in Equation (18).

$$\boldsymbol{v}_k = \frac{1}{\sqrt{N}}(W^{0k} \quad W^{1k} \quad W^{2k} \quad \cdots \quad W^{(N-1)k})' \quad k = 0,1,2,\dots,N-1 \tag{18}$$

The eigenvector matrix, $[\boldsymbol{V}]$, is defined as the sequential concatenation of eigenvectors, provided in Equation (19).

$$[\boldsymbol{V}] = [\boldsymbol{v}_0 \quad \boldsymbol{v}_1 \quad \boldsymbol{v}_2 \quad \cdots \quad \boldsymbol{v}_{(N-1)}] \tag{19}$$

The circulant matrix $[\boldsymbol{\alpha}]$ can be diagonalized by $[\boldsymbol{V}]$ as shown in Equation (20), where $[\boldsymbol{V}]^H$ is the Hermitian matrix of $[\boldsymbol{V}]$.

$$[\boldsymbol{\alpha}] = [\boldsymbol{V}]^H \, diag(\lambda_0 \quad \cdots \quad \lambda_{N-1})[\boldsymbol{V}] \tag{20}$$

The inverse of $[\boldsymbol{\alpha}]$ is developed as shown in Equation (21).

$$[\boldsymbol{\alpha}]^{-1} = [\boldsymbol{V}]^H diag(\frac{1}{\lambda_0} \quad \cdots \quad \frac{1}{\lambda_{N-1}})[\boldsymbol{V}] \tag{21}$$

The inverse matrix of $[\boldsymbol{\alpha}]$ is also a circulant matrix because it shares the eigenvectors of $[\boldsymbol{\alpha}]$ and the eigenvalue vector of $[\boldsymbol{\alpha}]^{-1}$ can be written as $\{\frac{1}{\lambda}\}$. Since the characterization vector $\{a\}$ is sparse, it is convenient to write the eigenvalues of $[\boldsymbol{\alpha}]$ as shown in Equation (22), where it can be seen that the eigenvalue vector $\{\lambda\}$ is symmetric (i.e., $\lambda_k = \lambda_{N-k}$, for $k = 1,2,\dots,N-1$).

$$\lambda_k = 1 + 2\alpha_1 cos\left(\frac{2\pi k}{N}\right) + 2\alpha_2 cos\left(\frac{4\pi k}{N}\right) \quad k = 0,1,2\dots N-1 \tag{22}$$

The characteristic vector of the inverse matrix, i.e. the first row of $[\boldsymbol{\alpha}]^{-1}$, is denoted as $\{\beta\}$. It can be obtained by performing an Inverse Discrete Fourier Transform to the eigenvalue vector of $[\boldsymbol{\alpha}]^{-1}$. The inverse matrix $[\boldsymbol{\alpha}]^{-1}$ also has a circulant form as shown by Equation (23), and is written as $\boldsymbol{B}$ for convenience.

$$[\boldsymbol{\alpha}]^{-1} = \boldsymbol{B} = Circ(\{\beta_i\})$$

$$\{\beta\} = [\beta_0, \beta_1, \beta_2, \dots, \beta_{N-2}, \beta_{N-1}] = \mathcal{F}^{-1}(\{\lambda_i^{-1}\}) \tag{23}$$

$$\beta_k = \frac{1}{N}\sum_{i=0}^{N-1}\frac{1}{\lambda_i}W^{-ik} \qquad k = 0,1,2,\dots,N-1$$

The characteristic vector $\{\beta\}$ is symmetric (i.e., $\beta_k = \beta_{n-k}, k = 1,2,\dots,N-1$) due to the symmetry of $\{\lambda\}$. Given Equation (16) and the symmetric property of $\{\beta\}$, the resultant deformed tire shape with one active segment is computed as Equation (24).

$$\{\boldsymbol{u}\} = \begin{bmatrix} \beta_0 & \beta_1 & \beta_2 & \beta_3 & \cdots & \beta_{n-2} & \beta_{n-1} \\ \beta_{n-1} & \beta_0 & \beta_1 & \beta_2 & \cdots & \beta_{n-3} & \beta_{n-2} \\ \beta_{n-2} & \beta_{n-1} & \beta_0 & \beta_1 & \vdots & \beta_{n-4} & \beta_{n-3} \\ \beta_{n-3} & \beta_{n-2} & \beta_{n-1} & \beta_0 & \cdots & \beta_{n-5} & \beta_{n-4} \\ \vdots & \vdots & \vdots & \vdots & \vdots & \vdots & \vdots \\ \beta_1 & \beta_2 & \beta_3 & \beta_4 & \cdots & \beta_{n-1} & \beta_0 \end{bmatrix} \begin{Bmatrix} \frac{f^a}{k_0} \\ 0 \\ \vdots \\ 0 \end{Bmatrix} = \frac{f^a}{k_0}\begin{Bmatrix} \beta_0 \\ \beta_1 \\ \beta_2 \\ \beta_3 \\ \vdots \\ \beta_{n-1} \end{Bmatrix} = \frac{f^a}{k_0}\{\beta\} \tag{24}$$

To summarize, the deformed tire shape vector $\{\boldsymbol{u}\}$ for a single active element is the vector $\{\beta\}$ scaled by $k_0^{-1}F^a$. The characteristic vector $\{\beta\}$ is obtained by calculating the Inverse Discrete Fourier Transformation of $\{\lambda_i^{-1}\}$, which is determined by the shape coefficients α_1 and α_2, as shown in Equation (17).

Spatial Frequency Constraints

There are two spatial frequency constraints placed on the tire shape. The first is that there is no single harmonic that dominates the shape. The second is that low order (low spatial frequency) components must contribute more than higher order components to the overall tire shape. Each of these constraints is developed in turn. First, it is clear from Equation (23) that if one of the eigenvalues of the shape matrix, say λ_m, approaches zero, then the characteristic vector $\{\beta\}$ would be dominated by the nearly infinite term β_m and the remaining components would be negligible. In this case, the deformed tire shape vector $\{u\}$ would be harmonic, resulting in an unrealistic deformed tire shape. Figure 3 shows examples of undesirable tire shapes that are dominated by a single harmonic term; the solid line represents the undeformed tire shape and the dashed lines represent the deformed tire shape with a dominant harmonic term. The first diagram, $m = 0$, shows the shape of a tire containing only a constant radial deformation (which violates the condition that perimeter is fixed – it is a steel band). The second diagram shows the condition for $m = 3$ in which the bottom of the tire is flat, but the upper-right and upper-left sections of the tire are also deflected inward, which is unreasonable. These shapes may correspond to components of free-vibration of a tire, but they fail to capture the deformed shape of a tire in quasi-static contact with the pavement. Therefore, since no single harmonic can dominat the shape, none of the eigenvalues of the shape matrix can approach zero; this first spatial frequency constraint is written as Equation (25) .

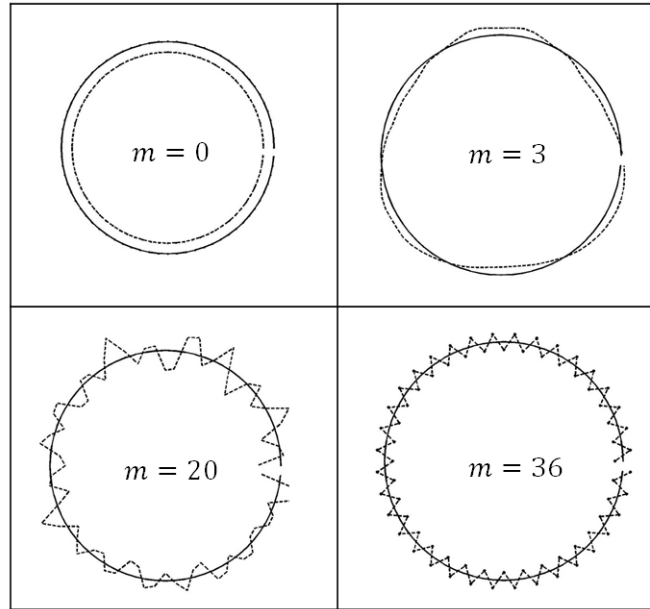$$\lambda_i \neq 0, \quad \forall i \in \{0,1,2 \ldots n-1\} \tag{25}$$

Figure 3. Solid line: Undeformed tire shape; Dashed line: deformed tire shape with dominant harmonic

It can be shown from Equation (22) that λ_i can be rewritten as a function of a new variable ξ as Equation (26).

$$\lambda_i(\xi) = 4\alpha_2\xi^2 + 2\alpha_1\xi + 1 - 2\alpha_2 \qquad i = 0,1,2 \ldots N-1 \tag{26}$$

$$\xi = \cos\left(\frac{2\pi k}{N}\right), \xi \in [-1,1]$$

Therefore, the constraint given in Equation (25) can be rewritten in terms of ξ as Equation (27).

$$\lambda_i(\xi) \neq 0, \forall \xi \in (-1,1) \tag{27}$$

Recall that the model is quasi-static and therefore the radial deformation vector should be dominated by a combination of low-order terms. Again, the deformation should not be dominated by a single harmonic. This low-order dominance is developed in mathematical terms by considering Equation (24) and noting that low-order tire shapes occur when the vector $\{\beta\}$ is dominated by low-order terms. Next consider Equation (23) and note that the

elements β_k that compose the vector $\{\beta\}$ are determined by the relative weighting term, $\frac{1}{\lambda_i}$, of the function $W^{-ik} = e^{\frac{2\pi ik}{N}j}$. Therefore, the weighting term $\frac{1}{\lambda_i}$ should be relatively large ($\lambda_i(\xi)$ should be small) in the low frequency range (i.e., $k \ll N/2$). This low frequency range corresponds to $\xi = 1$ as given by Equation (26). The weighting term should be relatively small ($\lambda_i(\xi)$ should be large) in the high frequency range (i.e., $k \approx N/2$) where $\xi = -1$. This second spatial frequency condition, the low frequency domination constraint, is therefore expressed as the inequality given in Equation (28)**Error! Reference source not found.**.

$$\lambda_i(1) < \lambda_i(-1) \tag{28}$$

Finally, note that the function $\lambda_i(\xi)$ is a parabola. Applying the constraint on α_2 that was derived in Equation (15), the constraint on the second derivative of $\lambda_i(\xi)$ is given in Equation (29).

$$\frac{d^2(\lambda_i(\xi))}{d\xi^2} = 8\alpha_2 = 8\frac{\gamma_1 N^3}{k_0} > 0 \tag{29}$$

That is, the parabolic function $\lambda_i(\xi)$ faces upwards. If the discriminant is negative, i.e. $\Delta = 4\alpha_1^2 - 16\alpha_2(1 - 2\alpha_2) < 0$, the parabolic function $\lambda_i(\xi)$ does not have any roots. If the discriminant is positive there are two roots and if it is equal to zero then there is one root. The three cases are developed as follows.

Case 1. Negative Discriminant $\Delta = 4\alpha_1^2 - 16\alpha_2(1 - 2\alpha_2) < 0$

In this case, the function $\lambda_i(\xi)$ has no roots and $\lambda_i(\xi) > 0, \forall \xi \in [-1,1]$. Therefore the constraint shown in Equation (25) must hold for all possible choices of k and N. Pairs of values of α_1 and α_2 that yield a negative determinant are sufficient to ensure that there is no single dominant harmonic in the quasi-static response. Specifically, the inequality in Equation (30) is a sufficient constraint.

$$\frac{\alpha_1^2}{\frac{1}{2}} + \frac{(\alpha_2 - \frac{1}{4})^2}{\frac{1}{16}} < 1 \tag{30}$$

Since $\lambda_i(\xi) > 0, \forall \xi \in [-1,1]$ and given the constraint that $\alpha_2 > 0$ (from Equation (15)), the low frequency domination constraint is derived from Equation (26) as Equation (31).

$$\alpha_1 < 0 \tag{31}$$

Case 2. Positive Discriminant $\Delta = 4\alpha_1^2 - 16\alpha_2(1 - 2\alpha_2) > 0$

In this case the function $\lambda_i(\xi)$ has two roots given by Equation (32) where $\xi_2 > \xi_1$ since $\alpha_1 < 0$ and $\alpha_2 > 0$.

$$\xi_1 = -\frac{\alpha_1 + \sqrt{\Delta}}{4\alpha_2}$$
$$\xi_2 = -\frac{\alpha_1 - \sqrt{\Delta}}{4\alpha_2} \tag{32}$$

The function $\lambda_i(\xi)$ for this case is shown in Figure 4 as an upward facing parabola. If no single harmonic is to dominate the tire shape, then according to Equation (27) there must be no roots within the domain of ξ. Therefore, the entire domain of $\xi \in (-1,1)$ must fall into one of three regions, as shown in Figure 4.
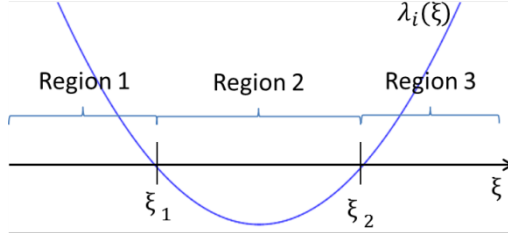
Figure 4. The function $\lambda_i(\xi)$ with discriminant $\Delta > 0$

In the first region, the entire domain of $\xi \in (-1,1)$ must be less than ξ_1 so that the inequality given in Equation (33) must hold.

$$1 < \xi_1 < \xi_2 \tag{33}$$

It follows from Equation (32) that the inequality expressed as Equation (34) must also be true.

$$\alpha_1 + 4\alpha_2 < -\sqrt{\Delta} < 0 \tag{34}$$

However, the inequality in Equation (34) contradicts the physical constraints expressed by Equation (15). Therefore Region 1 is not admissible.

In the second region, the entire range of $\lambda_i(\xi)$ must be negative so that the inequality given in Equation (35) must always hold.

$$\lambda_k(-1) < 0 \tag{35}$$

It follows from Equation (26) that this inequality is equivalent to Equation (36).

$$2\alpha_1 + 2\alpha_2 + 1 < 0 \tag{36}$$

The inequality in (36) contradicts the physical constraint expressed in (15). Therefore Region 2 is not admissible.

Finally, in the third region, the entire range of $\lambda_i(\xi)$ is monotonically increasing, so that the inequality given in Equation (33) must hold.

$$0 < \lambda_k(-1) < \lambda_k(1) \tag{37}$$

This inequality contradicts the low frequency domination constraint and therefore Region 3 is not valid. In summary, none of the three regions for the positive discriminant are admissible.

Case 3. Zero Discriminant $\Delta = 4\alpha_1^2 - 16\alpha_2(1 - 2\alpha_2) = 0$

Similar arguments can be made for the zero discriminant case as those made for the positive discriminant case. Here there is one root so that ξ_1 and ξ_2 are effectively equal and there are effectively two regions in Figure 4 to consider: Region 1 and Region 3. The conclusions for both of the regions are the same as in the case when the discriminant is positive. Therefore, the only case in which sufficient conditions to satisfy both spatial frequency constraints is when the discriminant is negative wherein the function $\lambda_i(\xi)$ has no roots and $\lambda_i(\xi) > 0, \forall \xi \in [-1,1]$.

Summary of Admissibility Constraints

All the active constraints on the shape coefficients α_1 and α_2 obtained under the three physical constraints and the two conditions derived from the spatial frequency constraints are expressed in Equation (38).

$$\begin{cases} 4\alpha_1^2 - 16\alpha_2(1 - 2\alpha_2) < 0 \\ \alpha_1 < 0 \\ \alpha_1 + 4\alpha_2 > 0 \end{cases} \tag{38}$$

Note that two of the five constraints are redundant. The resultant admissible region for α_1 and α_2 is plotted as Figure 5, with the white area denoting the admissible region.
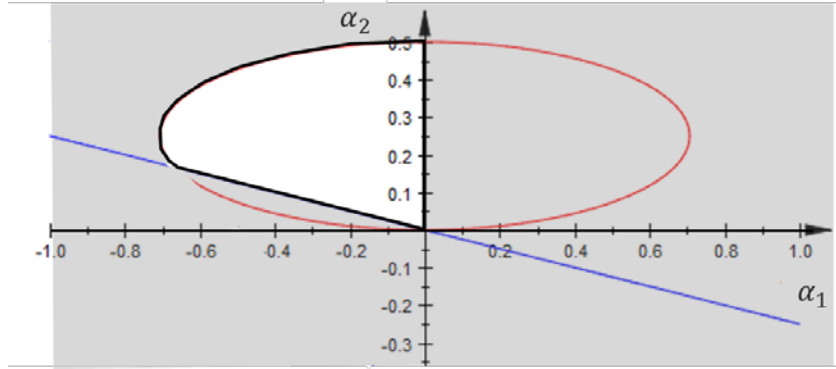

Figure 5. The admissible region for α_1 and α_2

EXPERIMENTAL VALIDATION

The experimental data used to validate this work is provided by Professor Schalk Els of the University of Pretoria, South Africa. The tire used is a Continental Conti-Trac AT 238/85 R16. Two quasi-static tests (a flat plate test and a cleat test) are performed that produce resultant spindle force, F, with respect to the tire deflection, e. The side length of the square tube is 19 mm. The stiffness, k_0, and shape parameters, α_1 and α_2, were tuned to approximate experimental results shown in Figure 5 and Figure 6. It must be noted that a more formal process to identify the best parameterization of the model is under development. In both figures the experimental results are shown as a solid line while the simulation results are shown as a dashed line. It is clear from Figure 5 that the nonlinear stiffening characteristic of the tire is captured by the constraint mode tire model as indicated by the increased slope with increasing deflection. The difference between the simulated and experimental forces is less than 4%.
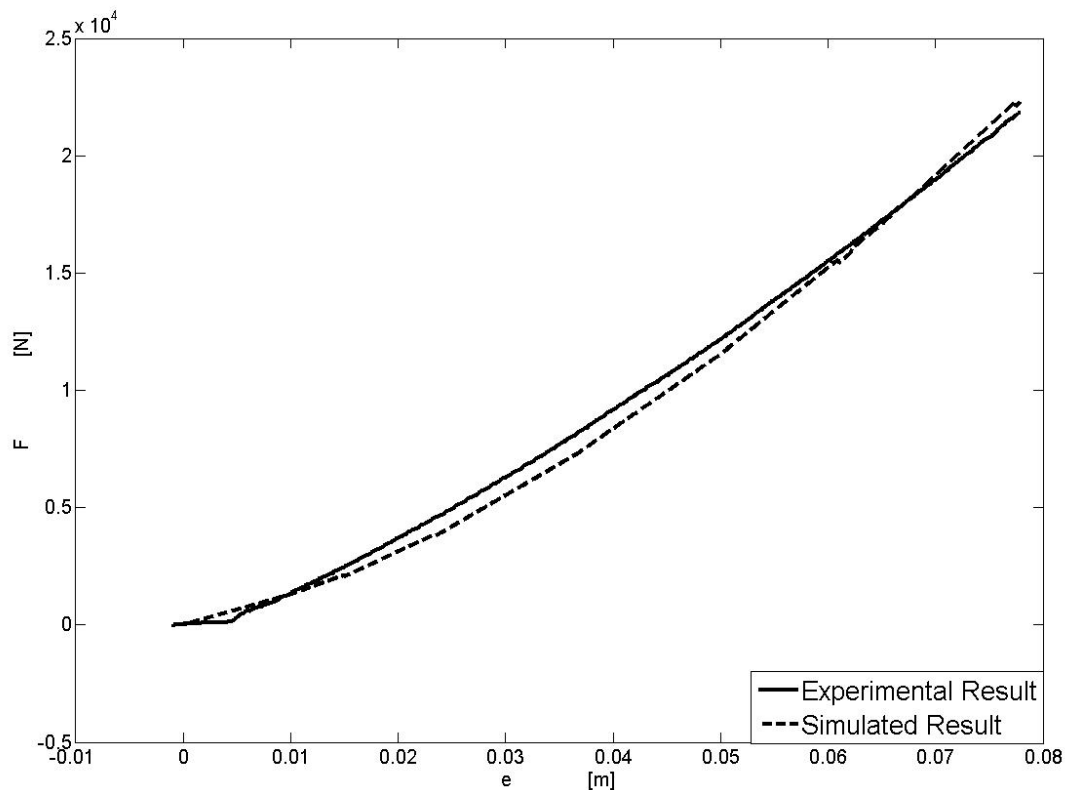
Figure 6. Flat-plate experimental and simulated force, *F*, with respect to the deflection, *e*

The cleat test results shown in Figure 6 show reasonable agreement throughout the range of deflection. It is clear that a discontinuity in stiffness occurs when the deflection exceeds approximately 5cm, dividing the results into two regions. In the first region (displacements up to 5cm) the tire is suspended by the cleat and the contact area related to force generation is constrained to the cleat surface only; the resulting stiffness is relatively small. This is shown conceptually in the upper inset picture in Figure 6. Here the difference between the experimental and simulated force data is less than 7%. In the second region the tire tread touches the surface below the cleat and the total contact area increases, as shown in the lower inset picture. This discontinuity in stiffness is captured by the constraint mode tire model. Note that although a simple linear model is used to predict the radial deflection of the tire surface, both of the nonlinear effects shown in Figure 5 and Figure 6 are captured.
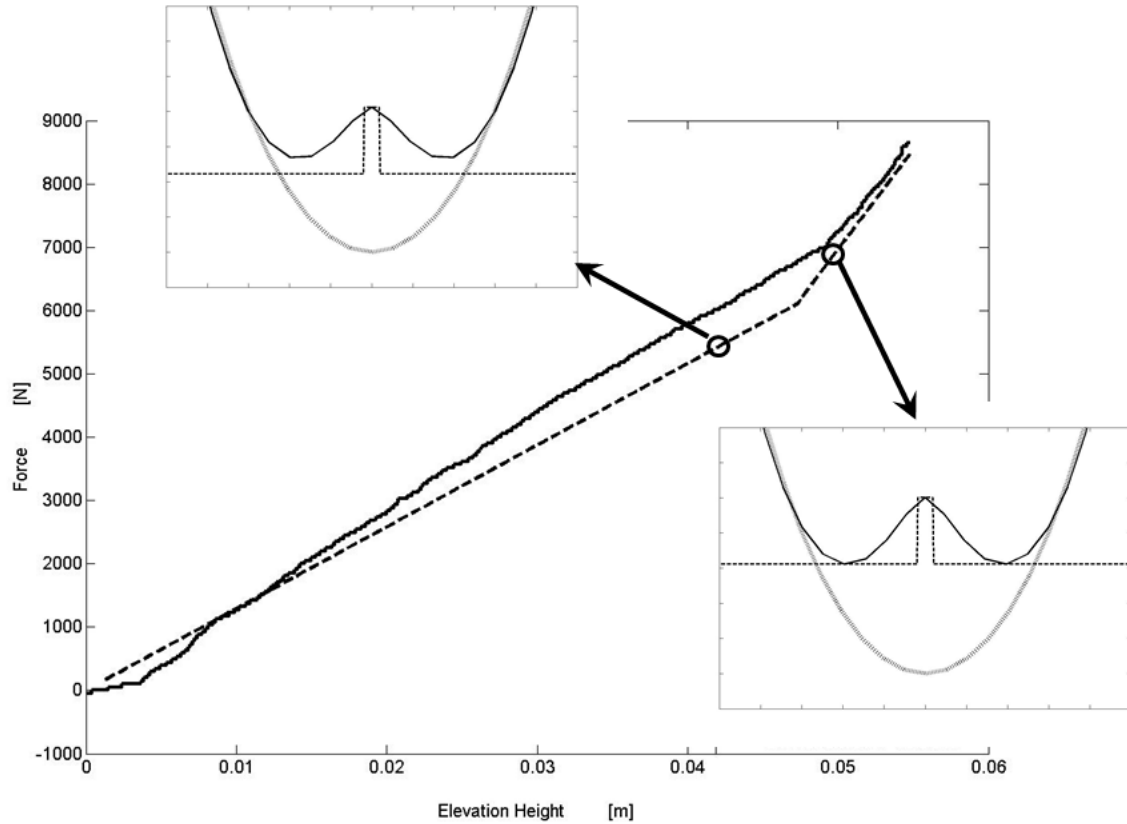
Figure 6. Cleat experimental and simulated force, *F*, with respect to the deflection, *e*

DISCUSSION

The two main contributions of this work are the description of the linear planar tire model in terms of a single stiffness parameter and two shape parameters and the development of an admissible region for the shape parameters. It is clear that the particular choice of tire parameters used in this work produces reasonable force predictions and accounts for nonlinear changes in stiffness. A parameterization process that more exactly replicates the experimental results for a particular tire is outside the scope of this work, but is the focus of future studies.

It is envisioned that the constraint mode tire model developed in this work can serve as a terrain morphological filter. That is, this constraint mode tire model can be used to pre-filter the terrain surface once, providing the required bridging and enveloping properties of the tire. A simpler tire model (perhaps a simple linear point-follower) could be used in the iterative design process to provide fast yet reliable spindle force prediction for vehicle dynamic simulation and reliability evaluation. Specifically, an effective road profile could be estimated given an actual terrain profile by simulating the constraint mode tire model traveling over an actual terrain profile given a constant spindle load. It is hoped that a small sacrifice in accuracy will results in an order of magnitude increase in computational speed. Ultimately, the tire constraint model will be further improved so that it can be applied to both deterministic terrain profiles and stochastic terrain profiles.

CONCLUSIONS

The first contribution of this work is a computationally efficient, planar, quasi-static, constraint mode tire model that captures the deformed tire shape. The required model parameters are reduced to two non-dimensional shape parameters and an overall stiffness factor. The second contribution is an admissible domain for the shape parameters that are sufficient to produce a realistic tire deflection. Although the focus of the work is to develop a simple linear model to predict the tire shape, simulated spindle loads are compared to experimental loads for a flat plate test and a

cleat test. The results of the experimental comparison demonstrate that nonlinear stiffness effects are adequately captured by this simple linear tire model. A computationally efficient, planar tire model that accurately predicts the lower-frequency, but not necessarily low amplitude, tire shape has been developed. This model strikes a balance between heuristic tire models (such as a linear point-follower) that lack the fidelity to make accurate chassis load predictions and computationally intensive models that cannot provide timely predictions. It is hoped that this tire model is used as an integral part of the computationally efficient and accurate vehicle dynamic simulations that are critical throughout the iterative design process.

ACKNOWLEDGEMENTS

REFERENCES

1. Aurell, J. and Edlund, S., 1989, "Operating Severity Distribution11th International Association of Vehicle System Dynamics Symposium (IAVSD 1989)

2. Umsrithong, A., Stochastic Semi-Empirical Transient Tire Models, in Mechanical Engineering. 2012, Virginia Tech: Blacksburg, VA.

3. Badalamenti, J.M.D., G. R., Radial-interradial Spring Tire Models, Acoustic, Stress and Reliability in Design. Journal of Vibration, 1988. 110(1): p. 70-75.

4. Zegelaar, P.W.A.P., H. B., The In-plane Dynamics of Tyres on Uneven Roads. Vehicle System Dynamics, 1996: p. 714-730

5. Loo, M., A Model Analysis of Tire Behavior under Vertical Loading and Straight-Line Free Rolling. Tire Science and Technology, 1985. 13(2): p. 67-90.

6. Gillespie, T.D., Fundamentals of Vehicle Dynamics. 1992, Warrendale, PA: Society of Automotive Engineers, Inc.

7. Takayama, M.Y., K., Simulation Model of Tire Vibration. Tire Science and Technology, 1984. 11(1): p. 38 – 49.

8. Ferris, J.B., Capturing Planer Tire Enveloping Properties Using Static Constraint Modes, in ASME 2006 International Mechanical Engineering Congress and Exposition (IMECE2006), Dynamic Systems and Control Division 2006: Chicago, Illinois, USA p. IMECE2006-15260 pp. 467-472

9. Guyan, R.J., Reduction of Stiffness and Mass Matrices. AIAA Jounrnal, 1965. 3(2): p. 380.

10. Ma, R., A.A. Reid, and J.B. Ferris. Capturing Plannar Tire Properties Using Static Constraint Modes. in ASME-DSCC. 2012. Ft. Lauderdale, FL.

11. Golub, G.H.V.L., Charles F., Matrix Computations Vol. 4.7.7 Circulant Systems. 1996: Johns Hopkins.